Monolayer II-VI semiconductors: A first-principles prediction

Hui Zheng,[1] Xian-Bin Li,[1,*] Nian-Ke Chen,[1] Sheng-Yi Xie,[1] Wei Quan Tian,[1,2] Yuanping Chen,[3] Hong Xia,[1] S. B. Zhang,[1,4,†] and Hong-Bo Sun[1,‡]

[1]*State Key Laboratory on Integrated Optoelectronics, College of Electronic Science and Engineering, Jilin University, Changchun 130012, China*

[2]*Institute of Theoretical Chemistry, Jilin University, Changchun 130012, China*

[3]*Laboratory for Quantum Engineering and Micro-Nano Energy Technology, Xiangtan University, Xiangtan 411105, China*

[4]*Department of Physics, Applied Physics, & Astronomy, Rensselaer Polytechnic Institute, Troy, New York 12180, USA*

(Received 11 January 2015; revised manuscript received 14 May 2015; published 21 September 2015)

A systematic study of 32 honeycomb monolayer II-VI semiconductors is carried out by first-principles methods. While none of the two-dimensional (2D) structures can be energetically stable, it appears that BeO, MgO, CaO, ZnO, CdO, CaS, SrS, SrSe, BaTe, and HgTe honeycomb monolayers have a good dynamic stability. The stability of the five oxides is consistent with the work published by Zhuang *et al.* [Appl. Phys. Lett. **103**, 212102 (2013)]. The rest of the compounds in the form of honeycomb are dynamically unstable, revealed by phonon calculations. In addition, according to the molecular dynamic (MD) simulation evolution from these unstable candidates, we also find two extra monolayers dynamically stable, which are tetragonal BaS [$P4/nmm(129)$] and orthorhombic HgS [$P2_1/m(11)$]. The honeycomb monolayers exist in the form of either a planar perfect honeycomb or a low-buckled 2D layer, all of which possess a band gap and most of them are in the ultraviolet region. Interestingly, the dynamically stable SrSe has a gap near visible light, and displays exotic electronic properties with a flat top of the valence band, and hence has a strong spin polarization upon hole doping. The honeycomb HgTe has recently been reported to achieve a topological nontrivial phase under appropriate in-plane tensile strain and spin-orbital coupling (SOC) [J. Li *et al.*, arXiv:1412.2528]. Some II-VI partners with less than 5% lattice mismatch may be used to design novel 2D heterojunction devices. If synthesized, potential applications of these 2D II-VI families could include optoelectronics, spintronics, and strong correlated electronics.

DOI: 10.1103/PhysRevB.92.115307 PACS number(s): 73.22.−f, 63.22.−m, 62.23.Kn, 78.55.Et

I. INTRODUCTION

In the past decade, the remarkable conductivity, strength, and other exotic electronic properties of graphene have made it a promising candidate for a stretchable transparent electrode [1], ballistic transistor [2], proposed nanospaser [3], platform for exploring gas separation properties [4], metamaterials [5], and other interesting physics [6,7]. While graphene is only a single layer with a potential to revolutionize electronics, it still has one critical limitation, i.e., it has no band gap. As such, even though graphene has very high carrier mobility, its field effect transistor (FET) has an especially low on/off ratio, compared to that of silicon based FET, which has no doubt to cost more energy in device applications. Therefore, new two-dimensional (2D) materials beyond graphene with well-defined band gap are highly desirable for future electronics.

Extensive efforts have been made to discover new 2D materials and their exotic properties [8–12]. Cahangirov *et al.* showed that low-buckled honeycomb silicene and germanene could be stable by first-principles calculations [13]. Recently, the two structures have been successfully produced on metal substrates by Wu *et al.* and Dávila *et al.* [14,15]. However, two such systems still have no well-defined band gap. Şahin *et al.* predicted 22 honeycomb structures mainly for group III-V compounds [16,17]. Among them, 2D boron nitride (BN) has been realized in experiment [18,19]. Single layer molybdenum disulfide (MoS_2) [20] and black phosphorus (*b*-P) [21] have also been synthesized. These structures (BN, MoS_2, *b*-P) are gaped: 6.07 eV for BN [22], 2.84 eV for MoS_2 [23], and 2.00 eV for *b*-P [24]. Most recently, Miao, based on proper electron counting, proposed a large family of 2D semiconductors [10]. While being very encouraging, clearly more such materials are required for full 2D electronic and optoelectronic applications.

Honeycomb is a simple 2D structure and has been popular for group IV elements (graphene, silicene, and germanene) and III-V compounds (BN). However, the 2D II-VI honeycomb has not yet been explored systematically for their structural stability, or their electronic and optoelectronic properties. In fact, traditional II-VI three-dimensional (3D) compounds have important applications in electronics and optoelectronics. For example, ZnO has the potential in blue-light devices [25], and ZnS is an important candidate for transmitting windows in the infrared region [26]. In this work, 32 2D honeycomb structures of IIA (or IIB)-VIA compounds are studied by first-principles calculations. Based on the calculated cohesive energy, the high-temperature molecular dynamics (MD) simulations, and phonon spectra, we suggest ten structures of relatively good stability (BeO, MgO, CaO, ZnO, CdO, CaS, SrS, SrSe, BaTe, and HgTe) to be worthy of experimental testing. The stability of the five oxides has also been examined by Zhuang *et al.* [27]. These 32 honeycomb 2D structures all have a band gap and most of them are suited for ultraviolet optoelectronics, as

*Corresponding author: lixianbin@jlu.edu.cn
†Corresponding author: zhangs9@rpi.edu
‡Corresponding author: hbsun@jlu.edu.cn

revealed by hybrid functional calculations. Most interestingly, SrSe not only has a good dynamic stability but also possesses a flat valence band, which becomes strongly spin polarized upon hole doping. These make the SrSe a high-potential contender to experimentally tryout in II-VI 2D materials. According to the MD simulation at 1000 K, the unstable honeycomb structure tends to form a four-member-ring structure, thus we explored a standard tetragonal structure [$P4/nmm(129)$] for all 32 kinds of compounds systematically and did find the 2D BaS monolayer dynamically stable. Inspired by the work of 2D HgO [27], we also find an orthorhombic HgS [$P2_1/m(11)$] dynamically stable. In addition, both the tetragonal BaS and orthorhombic HgS monolayer own indirect band gaps. Interesting properties and potential applications of the present II-VI semiconductors are discussed.

II. METHODS

The projector augmented wave (PAW) [28] method, as implemented in the VASP code [29] with a plane-wave energy cutoff of 500 eV, is employed and the density functional theory (DFT) within the local density approximation (LDA) [30] is used. For Brillouin zone (BZ) integration, the Monkhorst-Pack scheme [31] with a $(25 \times 25 \times 1)\,k$-point grid is used. The convergence criteria are 10^{-5} eV for energy and 10^{-4} eV/Å for force. For group IIB elements, the d electrons are also treated as valence electrons. The phonon calculations employ a supercell approach, as implemented in the Phonopy code [32], where the supercell contains $4 \times 4 \times 1$ primitive cells and the corresponding k-point sampling uses a $4 \times 4 \times 1$ grid. In the MD simulations, the temperature is kept at 1000 K for 10 ps with a time step of 2 fs. The Heyd-Scuseria-Ernzerhof (HSE)

TABLE I. Structure and physical properties of 32 2D II-VI semiconductors. a is the lattice parameter and $\mathbf{\Delta}$ is the buckling parameter, as defined in Fig. 1. d-2D and d-3D are the shortest bond lengths between two types of atoms, and E_c-2D and E_c-3D are the cohesive energies per formula unit in the 2D and 3D structures, formation energy $\delta E_c = E_c\text{-}3D - E_c\text{-}2D$, and D_n is the Pauling electronegativity difference. The corresponding 3D structures are also listed with RC, ZB, WZ, OT, and TR and stand for rock-salt, zinc blend, wurtzite, orthorhombic, and trigonal, respectively. Dynamic stability criteria is based on the phonon spectra in Figs. 4 and 5 with G and P for good and poor stability, respectively. The last column lists the positions of the VBM and CBM in the BZ zone, K, M, and Γ is the high-symmetry points in the first Brillouin zone of hexagonal lattice, while the P represents the particular point deviate slightly from Γ point along with the high-symmetry line.

Name	a (Å)	Δ (Å)	d-2D (Å)	d-3D (Å)	E_c-2D (eV)	E_c-3D (eV)	δE_c (eV)	D_n	3D structure	Dynamic stability	VBM-CBM
BeO	2.64	0	1.53	1.63	13.81	14.26	0.45	1.87	WZ	G	$K\Gamma$
MgO	3.24	0	1.87	2.07	10.59	11.83	1.24	2.13	RC	G	$K\Gamma$
CaO	3.69	0	2.13	2.35	11.33	12.83	1.50	2.44	RC	G	$M\Gamma$
SrO	3.98	0	2.30	2.54	10.45	11.85	1.40	2.49	RC	P	$K\Gamma$
BaO	4.26	0	2.46	2.74	10.41	11.53	1.12	2.55	RC	P	$K\Gamma$
ZnO	3.21	0	1.85	1.95	8.38	9.09	0.71	1.79	WZ	G	$\Gamma\Gamma$
CdO	3.59	0	2.07	2.33	6.88	7.86	0.98	1.75	RC	G	$\Gamma\Gamma$
HgO	3.67	0	2.12	2.05	5.07	5.79	0.72	1.44	OT	P	$P\Gamma$
BeS	3.41	0	1.97	2.08	9.70	10.35	0.65	1.01	ZB	P	KM
MgS	4.03	0	2.33	2.56	7.68	8.71	1.03	1.27	RC	P	$K\Gamma$
CaS	4.47	0	2.58	2.78	9.00	10.68	1.68	1.58	RC	G	$M\Gamma$
SrS	4.76	0	2.75	2.96	8.55	10.22	1.67	1.63	RC	G	$M\Gamma$
BaS	5.05	0	2.91	3.15	8.75	10.27	1.52	1.69	RC	P	$K\Gamma$
ZnS	3.80	0	2.19	2.30	6.68	7.40	0.72	0.93	ZB	P	$\Gamma\Gamma$
CdS	4.16	0	2.40	2.50	5.85	6.61	0.76	0.89	WZ	P	$\Gamma\Gamma$
HgS	4.18	0	2.42	2.41	4.63	5.17	0.54	0.58	TR	P	$P\Gamma$
BeSe	3.61	0	2.09	2.20	8.67	9.33	0.66	0.98	ZB	P	KM
MgSe	4.24	0	2.45	2.70	6.91	7.84	0.93	1.24	RC	P	$K\Gamma$
CaSe	4.67	0	2.70	2.89	8.29	9.93	1.64	1.55	RC	P	$K\Gamma$
SrSe	4.95	0	2.86	3.07	7.91	9.57	1.66	1.60	RC	G	$M\Gamma$
BaSe	5.24	0	3.03	3.26	8.18	9.75	1.57	1.66	RC	P	$K\Gamma$
ZnSe	3.99	0.18	2.31	2.42	5.95	6.68	0.73	0.90	ZB	P	$\Gamma\Gamma$
CdSe	4.32	0.31	2.51	2.61	5.31	6.08	0.77	0.86	WZ	P	$\Gamma\Gamma$
HgSe	4.35	0.38	2.54	2.63	4.23	4.80	0.57	0.55	ZB	P	$P\Gamma$
BeTe	3.97	0	2.29	2.41	7.45	8.16	0.71	0.53	ZB	P	KK
MgTe	4.60	0	2.66	2.76	5.91	6.70	0.79	0.79	WZ	P	$K\Gamma$
CaTe	5.04	0	2.91	3.10	7.30	8.87	1.57	1.10	RC	P	$K\Gamma$
SrTe	5.32	0	3.07	3.27	7.01	8.64	1.63	1.15	RC	P	$K\Gamma$
BaTe	5.61	0	3.24	3.45	7.36	8.95	1.59	1.21	RC	G	$K\Gamma$
ZnTe	4.29	0.37	2.50	2.60	5.17	5.89	0.72	0.45	ZB	P	$\Gamma\Gamma$
CdTe	4.59	0.46	2.69	2.78	4.74	5.47	0.73	0.41	ZB	P	$\Gamma\Gamma$
HgTe	4.61	0.48	2.70	2.80	3.87	4.45	0.58	0.10	ZB	G	$P\Gamma$

hybrid functional method [33,34] with 25% exact exchange is used to estimate the reasonable band gap.

III. ATOMIC STRUCTURE AND ENERGETIC STABILITY

Table I summarizes the geometrical parameters, defined in Fig. 1, for the 32 structures. The buckling parameter Δ measures the degree of the structure away from a planar honeycomb. All the 2D honeycomb structures are planar, except for IIB selenides and tellurides, where a small buckling is observed. While the exact reason for the buckling is unknown, it has something to do with the presence of valence d electrons in the IIB elements. Moreover, the buckling is correlated to the relatively softer lattice of the 2D IIB selenides and tellurides, as revealed by the generally smaller cohesive energy (E_c-2D in Table I) [16] and to the noticeably smaller difference in the electronegativity between IIB cation and anion (D_n in Table I).

Table I also lists the calculated cohesive energy (E_c) per formula unit, which for the 2D structures is always lower than that for the corresponding 3D structures. In addition, Table I calculates the cohesive energy difference $\delta E_c = E_c$-3D − E_c-2D. The δE_c here is equal to the concept of formation energy used in [35]. In general this is the energy cost to synthesize single-layer materials from their three-dimensional bulk counterparts. Lower formation energy indicates that the candidate single-layer material is more stable. With this conception, we have identified several honeycomb monolayer group II-VI compounds with a comparable low formation energy like BeO 0.45 eV and HgTe 0.58 eV per formula unit. As a comparison, the calculated δE_c is 1.52 eV per Si dimer for silicene and 1.98 eV per Ge dimer for germanene [13]. By this standard and the fact that substrate-supported silicene and germanene have been experimentally fabricated [14,15], it is likely that some of the 2D II-VI structures may also be fabricated on a substrate.

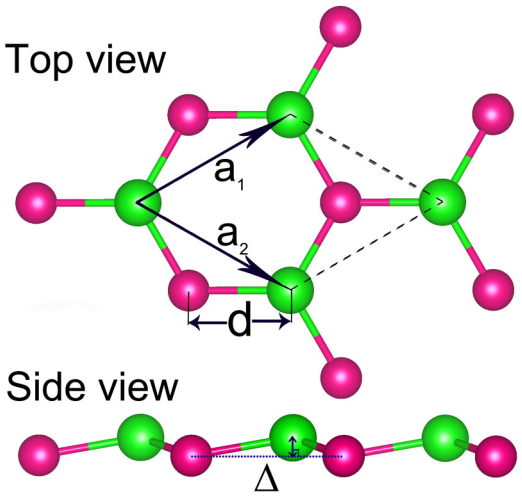

FIG. 1. (Color online) Schematic drawing of the graphenelike honeycomb structure for 2D II-VI semiconductors, where $\mathbf{a}_1$ and $\mathbf{a}_2$ are the corresponding lattice parameters, d is the shortest bond length between two types of atoms, and $\mathbf{\Delta}$ is the buckling parameter, which measures the vertical distances between a group II and a group VI atomic plane.

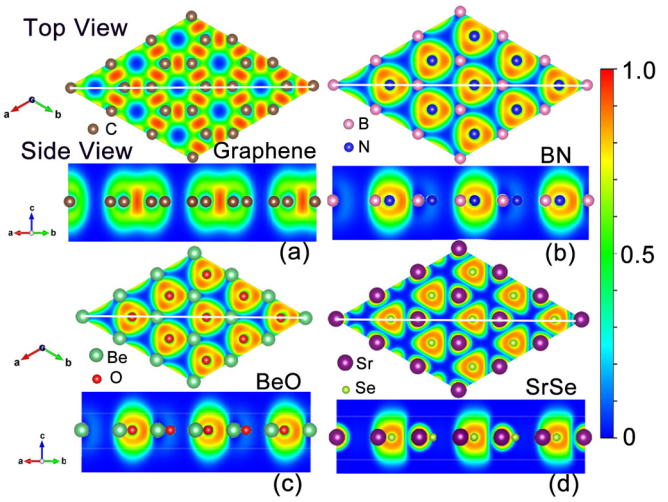

FIG. 2. (Color online) Top view and side view of the electron localization function (ELF) for graphene (a), BN (b), BeO (c), and SrSe (d), showing an ionic feature for II-VI 2D semiconductors. The white line in the top view defines the cross section for the side view.

Figure 2 shows the calculated electron localization function (ELF), which reveals the typical bonding characteristics for 2D group IV, III-V, and II-VI honeycomb semiconductors. The high electron density regions in graphene are usually located right in the middle between carbon atoms in plane, which indicates a strong nonpolar σ covalent bonding. It, however, gives way to ionic bonding even for the prototypical III-V BN, as well as for II-VI BeO and SrSe, demonstrated by the electron-location tendency to the atom with larger electronegativity. In addition, from the side view of ELF in graphene, the characteristic of π bonds (rendering by green color with ELF around 0.5) suspended upon the carbon atom plane is obvious. The picture reflecting the π bonds in graphene are much more diffused bonds than other localized bonds confined to the N atoms, O atoms and Se atoms, respectively, in BN, BeO, and SrSe honeycomb monolayer, correspondingly. The electronegativity difference of two types of elements in compounds of BN, BeO, and SrSe are 1.00, 1.87, and 1.60, respectively. Compared with the nonpolar covalent bonding in graphene where electrons are shared more equally, the larger the difference in electronegativity between the two types of atoms involved in the group II-VI compounds bonding, the more ionic (polar) they are, which corresponds to the much more localized ELF.

Despite the different bonding characteristics, the cohesive energy of the 2D structures are usually not small compared to that of group-IV counterparts, for example, the cohesive energy of BeO can be as large as 14 eV per formula unit. In accordance to their 3D bulk, the cohesive energy decreases from oxides to sulfides, to selenides, and to tellurides. Figure 3 shows the cohesive energy for the 2D structures as a function of the 2D lattice parameter. Interestingly, Mg always exhibits a pronounced minimum, which for Sr is, however, much less pronounced. While the cohesive energy of the IIB-VI compounds is noticeably smaller than that of the main group IIA-VI compounds, the values for Hg-VI semiconductors are exceptionally small.

Compared to the 3D structures, the 2D structures generally have shorter bond lengths (d-2D in Table I). It suggests

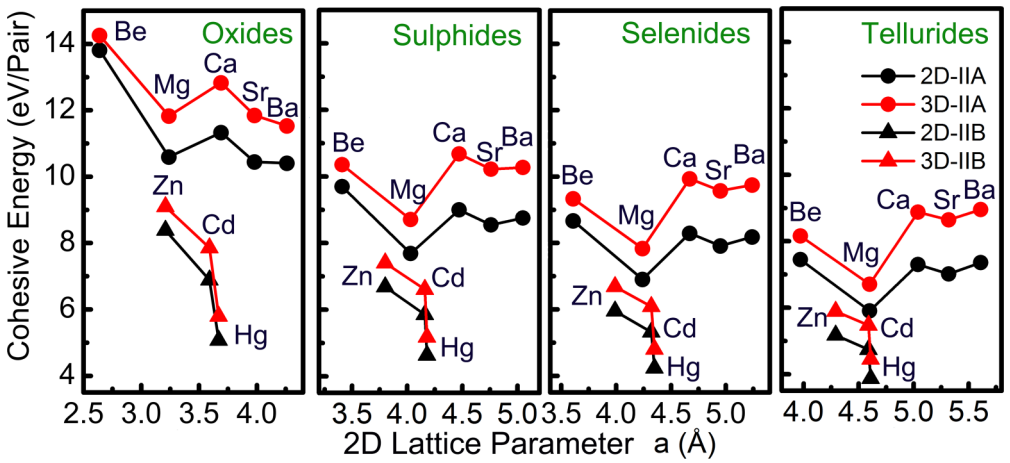

FIG. 3. (Color online) Calculated cohesive energy per formula pair of the 2D II-VI honeycomb semiconductors as the function of 2D lattice parameter.

that, in order to find a local energy minimum, these atoms in 2D structure favor to be close to each other, to achieve maximum orbital overlap so the bond distances are shorter. HgO is the exception because its 3D structure [*Pnma*(62)] simultaneously holds short (strong) bonds and long (weak) bonds other than the identical or quite similar bonds in

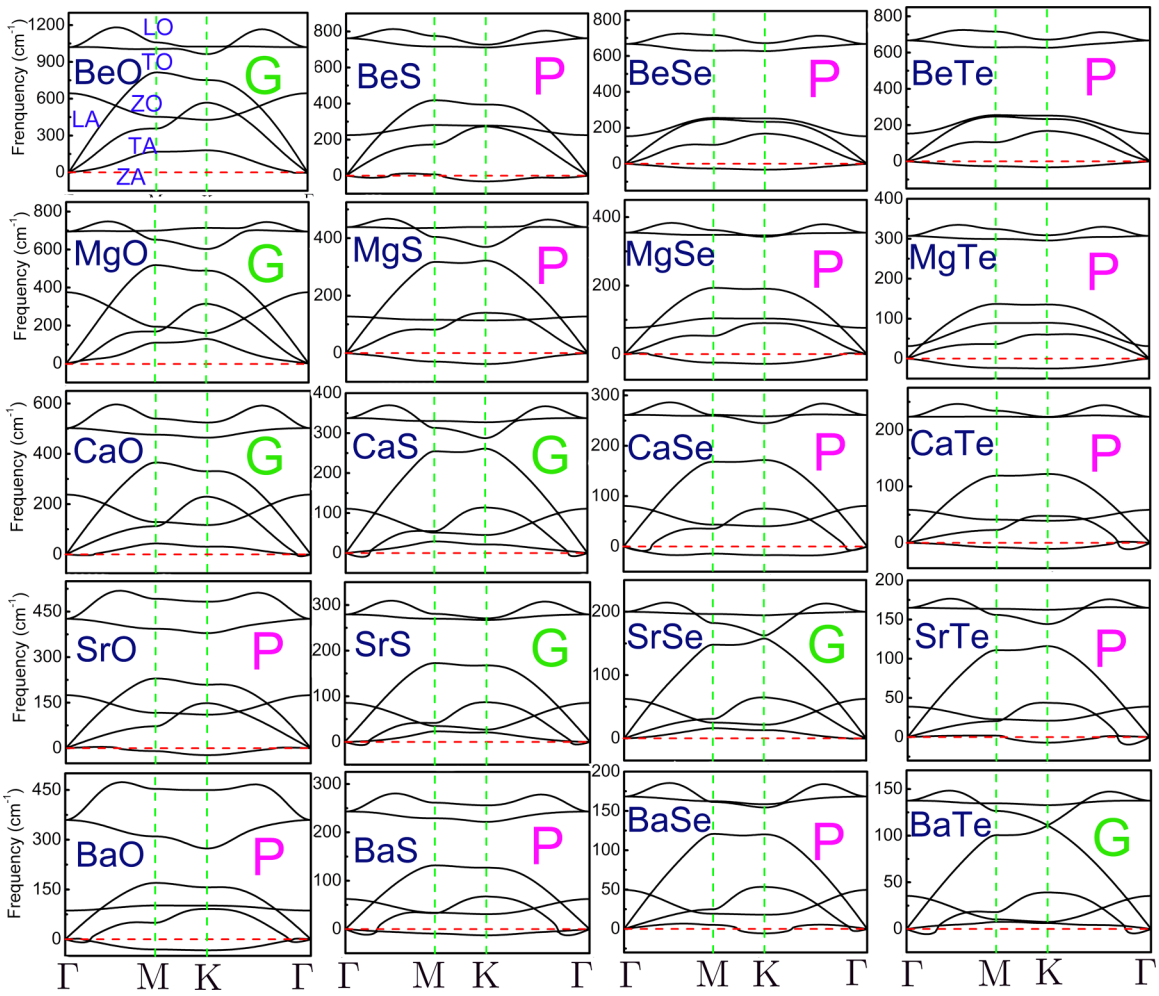

FIG. 4. (Color online) Phonon spectra for IIA-VI semiconductors. Letters G (green) and P (pink) are for good and poor dynamic stability, respectively. Red dashed line indicates zero frequency, below which the system becomes dynamically unstable. Without loss of generality, the phonon branches for BeO are labeled as ZA, TA, LA and ZO, TO, and LO. Z stands for vibrations in the z direction, notates the out-of-plane phonon modes, which are the most vulnerable modes for 2D systems.

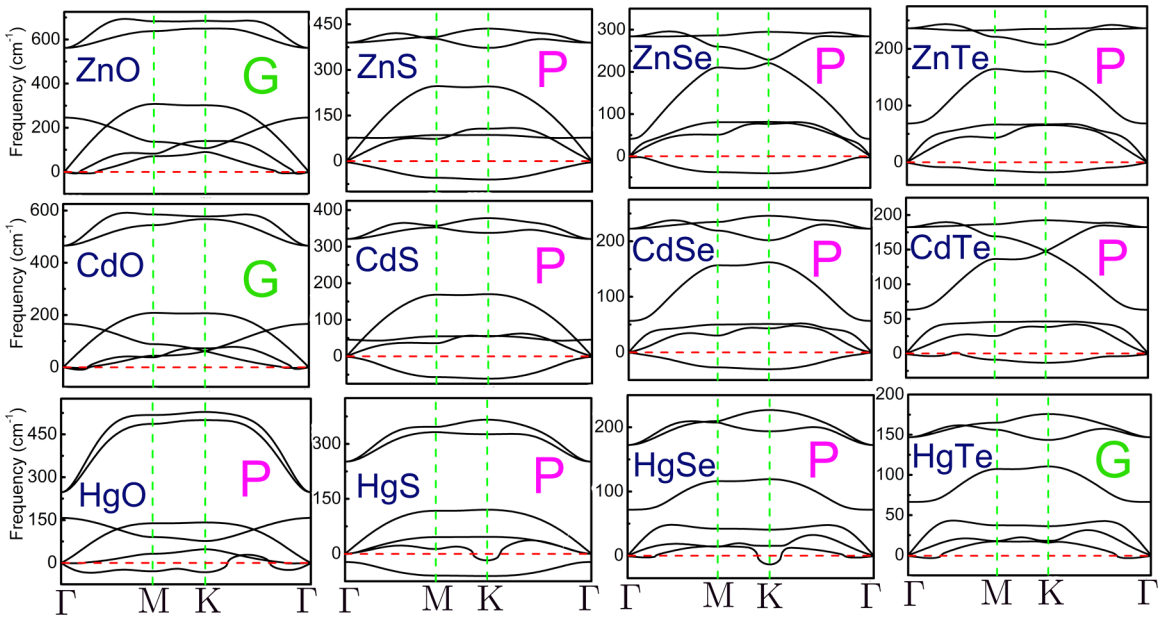

FIG. 5. (Color online) Phonon spectra for IIB-VI semiconductors. All legends are the same as in Fig. 4.

zinc-blend, wurtzite, or rock-salt structure. Although from the comparison of formation energy δE_c or cohesive energy of 2D and 3D identities, this is an energy cost process to synthesize monolayer materials from their three-dimensional bulk counterparts, the potential exotic qualities of 2D materials propel the desire to find these monolayer materials which are at a local minimum of potential energy surface rather than a saddle point [35]. This suggests that dynamic stability may be more relevant for fabricating this class of materials, provided that the materials have no imaginary phonon frequency (to be discussed below).

IV. PHONON SPECTRA, DYNAMIC STABLITY, AND STRUCTURE EVOLUTION

Figures 4 and 5 summarize the phonon spectra for 2D IIA- and IIB-VI semiconductors. Each of the II-VI honeycomb layers has three acoustic and three optical modes, denoted as ZA, TA, LA, and ZO, TO, LO, respectively, where Z stands for out-of-plane vibration along the z axis. Different from the 3D structures, one of the optical modes, i.e., the ZO mode, usually has significantly lower energy. In many cases, the ZO mode is even in the energy range of the TA and LA modes, leaving a noticeable gap with the other two optical phonon branches. As mentioned earlier, these dynamically stable monolayer candidates are at a local minimum of potential energy surface rather than at saddle point, which means their phonon modes must be real. Whereas imaginary phonon modes exhibit dynamic instability, on the other hand, also reflect the fact that these materials tend to transform into other possible structures like monolayer with ripples or say just different construction of atomic arrangement. As reported, ripples in graphene can occur due to strain or thermal fluctuations and stabilize the 2D material [36].

The results in the phonon spectra can be divided into two groups: *poor* dynamic stability when a majority of the ZA or ZO modes have an obvious imaginary frequency and *good* dynamic stability when essentially there is no imaginary frequency of any phonon branches. Our results show that BeO, MgO, CaO, ZnO, CdO, CaS, SrS, SrSe, BaTe, and HgTe honeycomb monolayers, in total ten kinds, have a good dynamic stability. The dynamic stability corroborates with the results of MD simulations at $T = 1000$ K in Fig. 6 for six typical 2D structures with *good* (BeO, MgO, ZnO, CaS) and *poor* (CdSe, HgS) dynamic stabilities.

At the end of the simulations, BeO, MgO, ZnO, and CaS basically only showed bond-length variation, which is characteristic of the harmonic oscillations whose amplitude increases from BeO to CaS. In the case of HgS, the noise level is so large that it surpasses most of the harmonic motion. Not surprisingly, after the 10-ps MD simulations, the honeycomb

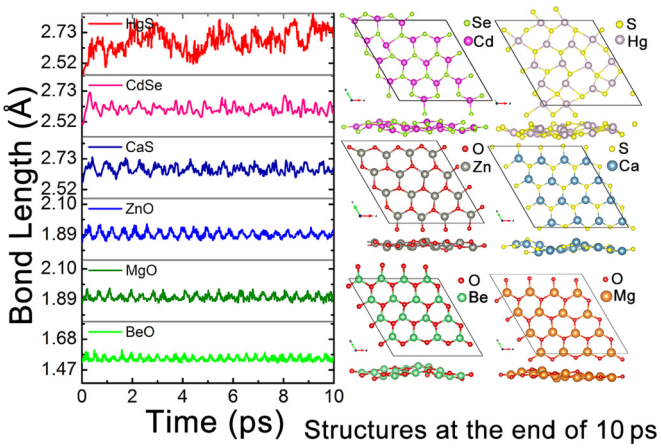

FIG. 6. (Color online) High-temperature annealing of six prototypical II-VI semiconductors. According to phonon modes, BeO, MgO, ZnO, CaS have good dynamic stability, and CdSe, HgS have relatively poor stability. The MD is done at $T = 1000$ K for 10 ps. The structures on the right panel are the snapshots after the 10-ps annealing.

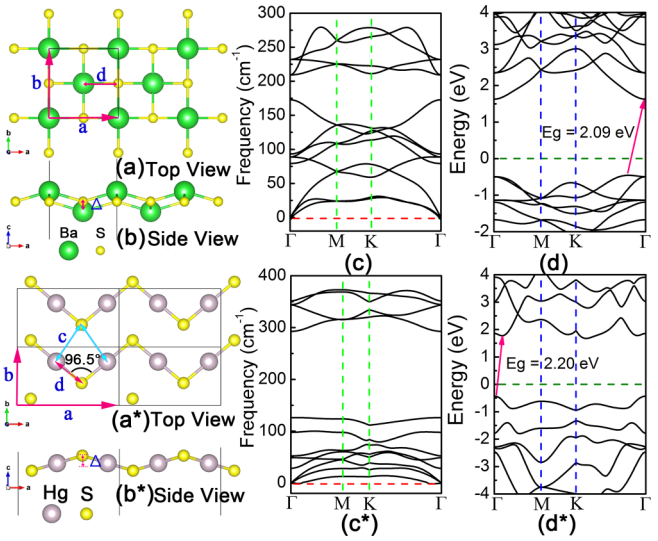

FIG. 7. (Color online) The tetragonal BaS and orthorhombic HgS. (a) and (b) and (a*) and (b*) are their top view and side view. For BaS, lattice parameter a equals b, which is 5.74 Å, the closest distance between different atoms d is 3.00 Å, the buckling parameter Δ is 0.85 Å. For HgS, a is 6.96 Å, b is 4.00 Å, the distance of Hg atoms and S atoms d (the short bond length) is 2.33 Å, c (the long bond length) is 3.12 Å, buckling parameter Δ is 0.52 Å. (c) and (c*) Their phonon spectra without imaginary frequency. (d) and (d*) The LDA band structures.

structure of HgS has been destroyed, resulting in the formation of four-membered rings. Interestingly, no five-membered rings are observed; in other words, the II-VI semiconductors have a natural tendency to prevent the formation of wrong (II-II or VI-VI) bonds. If one combines both the energetic and dynamic stabilities, BeO may be the most experimentally achievable 2D II-VI semiconductor. A former work [27] also showed that the BeO has the lowest formation energy corresponding to the bulk phase in the 2D hexagonal oxides. Apart from our research on the systematic honeycomb (hexagonal) monolayer of group II-VI, we get inspired by the HgS MD structure evolution and enlightened from the work by Hennig *et al.* [17,27,36], we also found the other two compounds with tetragonal and orthorhombic monolayer constructions dynamically stable: tetragonal BaS and orthorhombic HgS monolayer. Their crystal structures and dynamically stable phonon spectra are presented in Figs. 7(a)–7(c) and 7(a*)–7(c*). The space group of 2D tetragonal crystal structure of BaS is $P4/nmm(129)$, and that of 2D orthorhombic HgS is $P2_1/m$ (11). Considering their most stable 3D counterparts, the 2D tetragonal structure of BaS is just the layer exfoliated along the [001] direction of its rock-salt 3D structure [$Fm\bar{3}m(225)$]. However, the honeycomb BaS can be viewed as the atomic rearrangement along the [111] direction of bulk rock-salt BaS. In addition, we found an interesting law that generally speaking if the bulk structure of group II-VI materials own a rock-salt structure, the energy of the 2D tetragonal structure is lower than the corresponding 2D hexagonal structure. This law can be considered together with phonon for 2D material design.

The new founding 2D HgS is also related to its 3D counterpart or the sibling 3D HgO structure. Inspired by the previous work [27], they show that 2D HgO can transform into the structure with the space group [$Pbam$ (55)]. The reconstructed single layer HgO can be view as the cleaved atomic layer from the 3D bulk HgO [$Pnma$ (62)] along the [010] direction. Here the dynamically stable HgS [$P2_1/m(11)$] (we found) can be produced simply through anion buckling in cation plane based on the 2D HgO structure, see Figs. 7(a*) and 7(b*). Interesting, such 2D HgS has two short bonds (2.33 Å) and two long bonds (3.12 Å). Considering short bonds only, the 2D structure is composed by a series of *zigzag*-atom chains. This is somehow similar to the bulk structure of α-HgS [$P3_221(154)$] with a series of helix-atom chains. With consideration of both short and long bonds, the four-member-ring structure can be identified. This characteristic is somehow in accordance with the evolution structure with a significant amount of four-member rings after the 1000 K annealing as stated before. The cohesive energy of this newfound 2D HgS is 4.76 eV per pair, the formation energy (δE_c) is 0.41 eV per pair, which means its energy is quite close to that of its 3D counterpart, indicating good stability like the case of 2D BeO ($\delta E_c = 0.45$ eV per pair).

V. ELECTRONIC PROPERTIES

Figures 8 and 9 present the electronic band structures for 2D IIA-VI and IIB-VI semiconductors. In contrast to the case of graphene with a Dirac cone around Fermi level, most of the 2D II-VI semiconductors have a noticeably large band gap, except those materials composed of Hg element. Compared to the cases of graphene and other IV honeycomb structures, such exceptionally large band gaps are from the very large ionicity in the II-VI system. With the stronger the ionicity, the valence electrons are more localized around the anion atoms and off the cation atoms. This makes them possibly as a high permittivity gate dielectric material for future nanoscale FET. For all of these honeycomb monolayer materials, the p_z orbitals of the occupied bands are predominately located on the anion atoms. In other words, the sixfold symmetry of a honeycomb structure is broken due to the asymmetry of the A/B sublattices. It leads to the rehybridization of the valence and conduction band states and the elimination of the electronic degeneracy at the K point of the BZ [37]. Thus, it may be desirable to use 2D II-VI semiconductors for FET-based electronics or optoelectronics.

Among all the II-VI honeycomb structures, 29 of them have their conduction band minimum (CBM) located at the BZ center (i.e., the Γ point). Only BeS, BeSe, and BeTe have their CBM at either the M or K point. The valence band maximum (VBM) of the 2D IIA-VI semiconductors are usually located at the M or K point. Zn and Cd are the exceptions with their VBMs at the Γ point, forming direct-gap semiconductors. Among the main-group 2D IIA-VI semiconductors, only BeTe has a direct gap. The band structures of heavy-Hg-involving 2D structures are calculated with spin-orbit coupling (SOC). The band gaps appear to be small, 0.04–0.34 eV in the LDA and their dispersions resemble that of 2D topological insulators (TI). To be certain, however, one needs to calculate the $\mathbb{Z}_2$ topological invariant or edge state. Interestingly, such a work has just recently reported [38] that the low-buckled (LB) hexagonal monolayer of HgTe (as the same structure found in this work) can undergo a transition to a topological

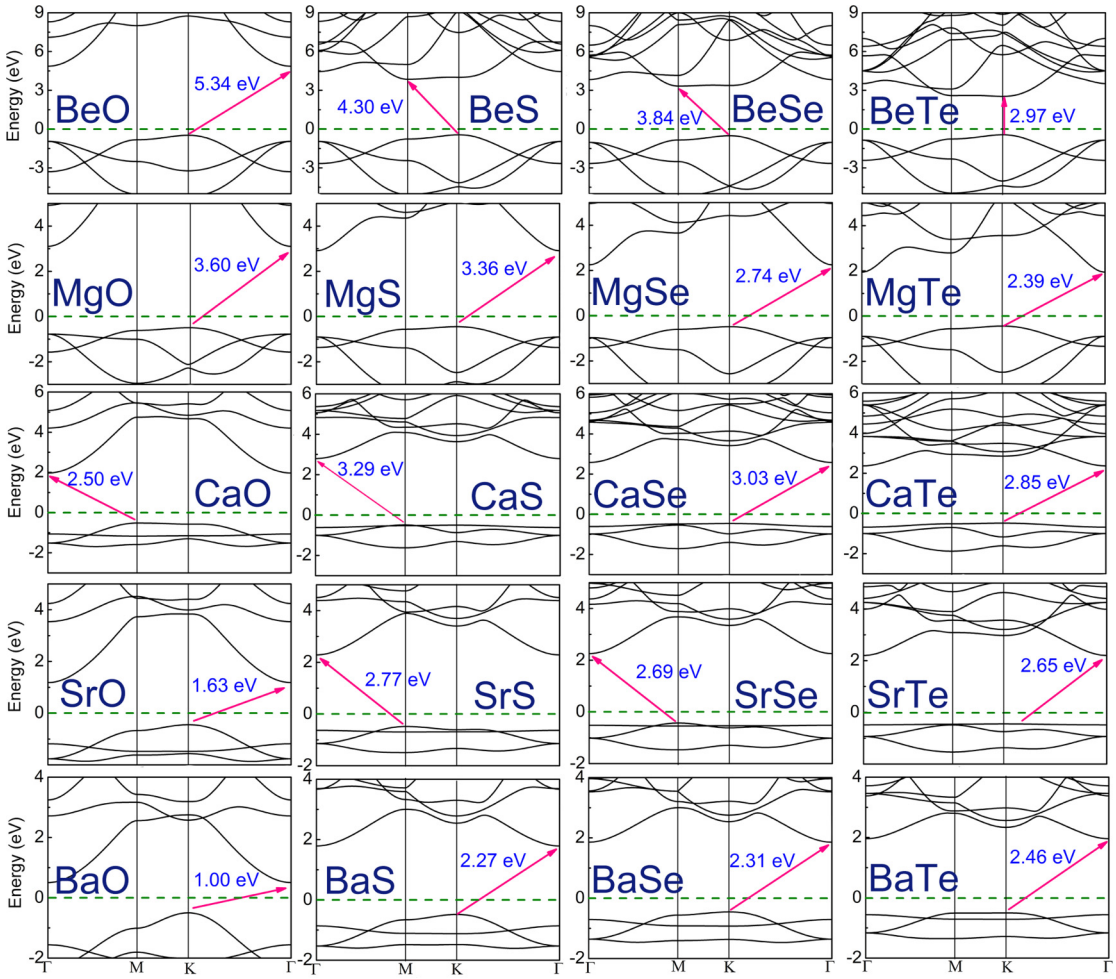

FIG. 8. (Color online) LDA band structures for 2D IIA-VI semiconductors with honeycomb structure. The relationship between VBM and CBM is indicated by a red arrow and the gap value is also given.

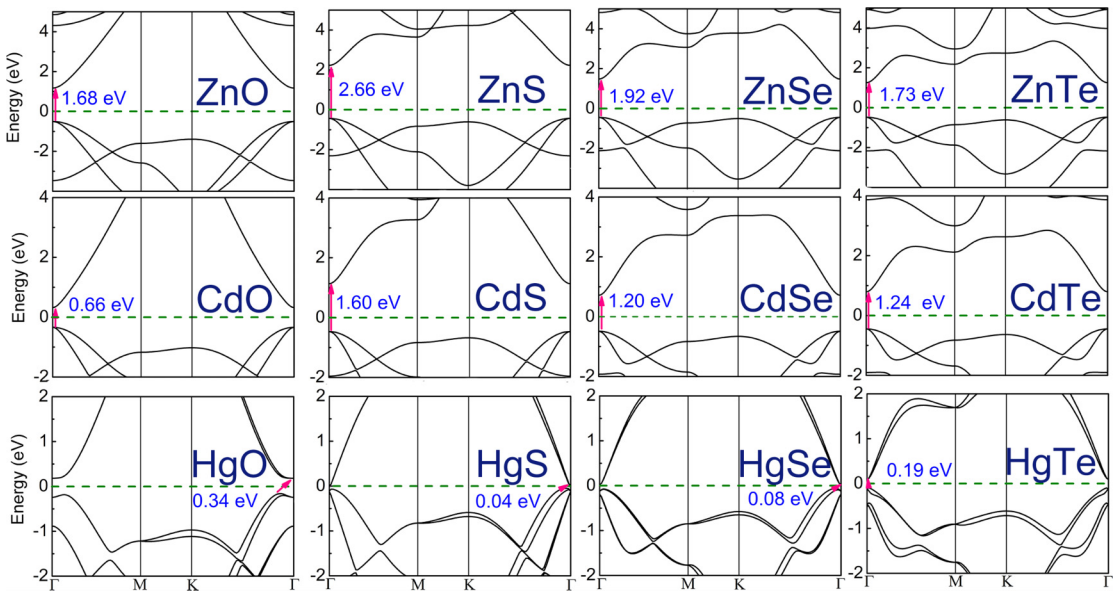

FIG. 9. (Color online) LDA band structures for 2D IIB-VI semiconductors with honeycomb structure. For the heavy element Hg, spin-orbital coupling (SOC) has been included. All legends are the same as in Fig. 8.

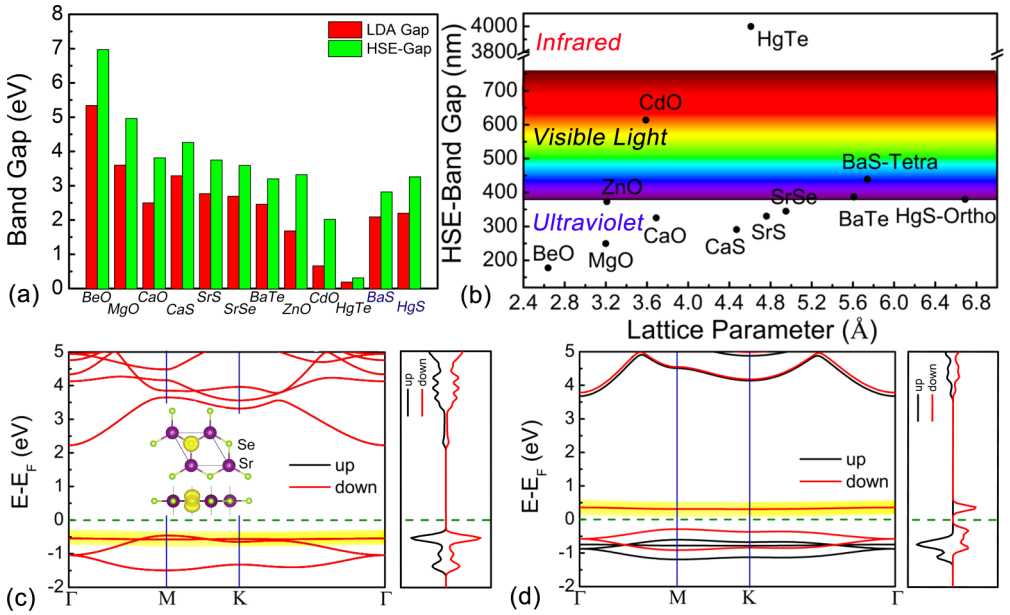

FIG. 10. (Color online) (a) Band gap for ten 2D hexagonal II-VI semiconductors as well as the extra BaS and HgS, with good dynamic stability, by both LDA and HSE calculation. (b) Optical wavelength corresponding to the HSE gaps as a function of the lattice parameters. (c) Spin-resolved LSDA band structure and the corresponding density of states (DOS) for SrSe. In the ground state, SrSe is nonmagnetic. Insets are the charge density distribution (both top and side views) of the (flat) topmost valence band (highlighted by yellow color). (d) Same as in (c) except one electron is subtracted from the topmost band (and equal to empty the band). As the band (highlighted by yellow color) becomes empty, it pops up to above the Fermi level, so the system becomes strongly ferromagnetic.

nontrivial phase under the appropriate in-plane tensile strain and spin-orbital coupling (SOC). For example, the in-plane tensile strain of $2.6\% < \varepsilon < 4.2\%$ and SOC together induce the band inversion and topological nontrivial gap. For $\varepsilon > 4.2\%$, the band inversion is already realized just by strain but the appearance of a topological gap still further needs SOC. The band gap of 2D-LB HgTe TI phase can be tuned over a wide range from 0 to 0.2 eV as the tensile strain increases from 2.6% to 7.4% [38]. In addition, the new found BaS and HgS are both the indirect band-gap semiconductors, as indicated in Figs. 7(d) and 7(d*).

The band gaps for the ten 2D honeycombs plus two extra BaS and HgS structures, which are stable at least dynamically, are evaluated with further HSE hybrid functionals [33,34]. Figure 10(a) compares them with LDA results. While the HSE gaps are noticeably larger than the LDA gaps, the percentage correction is smaller than what usually is for their 3D counterpart. Figure 10(b) shows that most of these materials are in the ultraviolet wavelength region, with the exception of CdO being in the visible red color, BaS in the blue color, and HgTe in the mid-IR region. Typically such 2D II-VI semiconductors are thus ultraviolet materials for UV-LED, UV-detector, or UV-LASER.

Finally, it appears that the 2D Ca-, Sr-, and Ba-VI semiconductors exhibit a flat top of the valence band. In particular, the dynamically stable SrSe also shows a rather flat top valence band with little k dependence [see the detailed band structure near the Fermi level in Fig. 10(c)]. For such a flat band, Coulomb interaction becomes important [39], which can be ideal for ferromagnetism and superconductivity [40]. Insets in Fig. 10(c) show the real-space charge distribution for the flat band, which has a p_z-orbital characteristic. It is found by a spin-polarized calculation that a strong ferromagnetism will result when one electron is subtracted from the primitive cell of SrSe, which is equal to empty the top valence band by adding lots of holes.

VI. LATTICE MISMATCH FOR HETEROJUNCTION

The P-N junction is one of the fundamental building blocks for modern electronics. With recent discoveries of atomically thin materials, layer-by-layer stacking (vertically stacked) or lateral interfacing (in-plane interconnected) heterojunction has been reported [41–43], which indicates the traditional semiconductor devices can be scaled down to atomic thicknesses. Table II summarizes the possible partners of the present finding II-VI semiconductors with lattice mismatch less than 5% for a

TABLE II. Possible candidates with small lattice mismatch for heterojunction. The lattice mismatch is defined as $|\frac{2(L_A-L_B)}{(L_A+L_B)}| \times 100\%$, L_X is the lattice constant for compound X. The mismatch $< 5\%$ could be possible for the stacked heterojunction in terms of the potential van der Waals connection [44]. The mismatch for MgO/ZnO is especially small ($< 1\%$) with indication of their possible lateral heterojunction.

A/B	L_A/L_B (Å)	Lattice mismatch
MgO/ZnO	3.24/3.21	0.93%
CaO/CdO	3.69/3.59	2.75%
CaS/HgTe	4.47/4.61	3.08%
SrS/SrSe	4.76/4.95	3.91%
SrS/HgTe	4.76/4.61	3.20%

potential stacked heterojunction device. Especially, the small mismatch (<1%) between ZnO and MgO may be even suitable for lateral heterojunction.

VII. CONCLUSION

In summary, 32 2D honeycomb single layer II-VI semiconductors have been investigated by first-principles calculations. There are at least ten kinds of hexagonal monolayer exhibiting promising dynamic stability: namely, BeO, MgO, CaO, ZnO, CdO, CaS, SrS, SrSe, BaTe, and HgTe. From the structure evolution of MD simulation and inspiration of former works, another two dynamically stable monolayer BaS [$P4/nmm(129)$] and HgS [$P2_1/m(11)$] have also been discovered. All the founded 2D II-VI semiconductors have a band gap, but most of them are in the ultraviolet wavelength region. Some of the 2D II-VI semiconductors also exhibit a flat top of valence band. In the case of SrSe, it is shown that a strong spin polarization and ferromagnetism will result due to hole doping. The low-buckled hexagonal HgTe monolayer may also realize a topological nontrivial phase under the appropriate in-plane tensile strain and spin-orbital coupling [38]. Small lattice mismatching partners may be suitable for heterojunction devices. The present systematic study reveals the families of II-VI 2D semiconductors with plenty of fascinating properties, which could be applied to future optoelectronic, nanoelectronics, and spintronics.

ACKNOWLEDGMENTS

The work was supported by the National Basic Research Program of China (Grant No. 2014CB921303), the National Natural Science Foundation of China (Grants No. 11374119, No. 61307119, and No. 61235004), and by the China Postdoctoral Science Foundation (Grant No. 2013T60315). S.B.Z. was supported by the Department of Energy under Grant No. DE-SC0002623. The High Performance Computing Center (HPCC) at Jilin University was acknowledged for calculation resources. W.Q.T. thanks for support from the Open Project of State Key Laboratory of Supramolecular Structure and Materials (JLU) (SKLSSM2015018).

[1] T. Chen, Y. Xue, A. K. Roy, and L. Dai, ACS Nano **8**, 1039 (2014).
[2] V. E. Calado, S. E. Zhu, S. Goswami, Q. Xu, K. Watanabe, T. Taniguchi, G. C. A. M. Janssen, and L. M. K. Vandersypen, Appl. Phys. Lett. **104**, 023103 (2014).
[3] V. Apalkov and M. I. Stockman, Light Sci. Appl. **3**, e191 (2014).
[4] S. Jungthawan, P. Reunchanc, and S. Limpijumnong, Carbon **54**, 359 (2013).
[5] N. Papasimakis, S. Thongrattanasiri, N. I. Zheludev, and F. J. García De Abajo, Light Sci. Appl. **2**, e78 (2013).
[6] L. Jiang, G. Yu, W. Gao, Z. Liu, and Y. Zheng, Phys. Rev. B **86**, 165433 (2012).
[7] L. Jiang, Y. Zheng, C. Yi, H. Li, and T. Lü, Phys. Rev. B **80**, 155454 (2009).
[8] S. Zhao, Z. Li, and J. Yang, J. Am. Chem. Soc. **136**, 13313 (2014).
[9] S.-Y. Xie, X.-B. Li, W. Q. Tian, N.-K. Chen, X.-L. Zhang, Y. Wang, S. Zhang, and H.-B. Sun, Phys. Rev. B **90**, 035447 (2014).
[10] M.-S. Miao, J. Botana, J. Liu, and W. Yan, arXiv:1503.00181.
[11] H. Tang and S. Ismail-Beigi, Phys. Rev. Lett. **99**, 115501 (2007).
[12] X. Y. Zhou, R. Zhang, J. P. Sun, Y. L. Zou, D. Zhang, W. K. Lou, F. Cheng, G. H. Zhou, F. Zhai, and K. Chang, Sci. Rep. **5**, 12295 (2015).
[13] S. Cahangirov, M. Topsakal, E. Aktürk, H. Şahin, and S. Ciraci, Phys. Rev. Lett. **102**, 236804 (2009).
[14] B. Feng, Z. Ding, S. Meng, Y. Yao, X. He, P. Cheng, L. Chen, and K. Wu, Nano Lett. **12**, 3507 (2012).
[15] M. E. Dávila, L. Xian, S. Cahangirov, A. Rubio, and G. Le Lay, New J. Phys. **16**, 095002 (2014).
[16] H. Şahin, S. Cahangirov, M. Topsakal, E. Bekaroglu, E. Akturk, R. T. Senger, and S. Ciraci, Phys. Rev. B **80**, 155453 (2009).
[17] H. L. Zhuang, A. K. Singh, and R. G. Hennig, Phys. Rev. B **87**, 165415 (2013).
[18] N. Alem, R. Erni, C. Kisielowski, M. D. Rossell, W. Gannett, and A. Zettl, Phys. Rev. B **80**, 155425 (2009).
[19] W. Auwärter, H. U. Suter, H. Sachdev, and T. Greber, Chem. Mater. **16**, 343 (2004).
[20] B. Radisavljevic, A. Radenovic, J. Brivio, V. Giacometti, and A. Kis, Nat. Nanotechnol. **6**, 147 (2011).
[21] W. L. Lu, H. Y. Nan, J. H. Hong, Y. M. Chen, C. Zhu, Z. Liang, X. Y. Ma, Z. H. Ni, C. H. Jin, and Z. Zhang, Nano Res. **7**, 853 (2014).
[22] K. K. Kim, A. Hsu, X. Jia, S. M. Kim, Y. Shi, M. Hofmann, D. Nezich, J. F. Rodriguez-Nieva, M. Dresselhaus, T. Palacios, and J. Kong, Nano Lett. **12**, 161 (2012).
[23] D. Y. Qiu, F. H. da Jornada, and S. G. Louie, Phys. Rev. Lett. **111**, 216805 (2013).
[24] V. Tran, R. Soklaski, Y. Liang, and L. Yang, Phys. Rev. B **89**, 235319 (2014).
[25] A. Tsukazaki, M. Kubota, A. Ohtomo, T. Onuma, K. Ohtani, H. Ohno, S. F. Chichibu, and M. Kawasaki, Jpn. J. Appl. Phys. **44**, L643 (2005).
[26] J. S. Mccloy, R. Korenstein, and B. Zelinski, J. Am. Ceram. Soc. **92**, 1725 (2009).
[27] H. L. Zhuang and R. G. Hennig, Appl. Phys. Lett. **103**, 212102 (2013).
[28] P. E. Blöchl, Phys. Rev. B **50**, 17953 (1994).
[29] G. Kresse and J. Furthmuller, Phys. Rev. B **54**, 11169 (1996).
[30] D. M. Ceperley and B. J. Alder, Phys. Rev. Lett. **45**, 566 (1980).
[31] H. J. Monkhorst and J. D. Pack, Phys. Rev. B **13**, 5188 (1976).
[32] A. Togo, F. Oba, and I. Tanaka, Phys. Rev. B **78**, 134106 (2008).
[33] A. V. Krukau, O. A. Vydrov, A. F. Izmaylov, and G. E. Scuseria, J. Chem. Phys. **125**, 224106 (2006).
[34] J. Heyd and G. E. Scuseria, J. Chem. Phys. **121**, 1187 (2004).
[35] H. L. Zhuang and R. G. Hennig, Jom **66**, 366 (2014).
[36] A. K. Singh and R. G. Hennig, Phys. Rev. B **87**, 094112 (2013).
[37] S. Y. Zhou, G. H. Gweon, A. V. Fedorov, P. N. First, W. A. De Heer, D. H. Lee, F. Guinea, A. H. Castro Neto, and A. Lanzara, Nat. Mater. **6**, 770 (2007).

[38] Jin Li, C. He, L. Mneg, H. Xiao, C. Tang, X. Wei, N. Kioussis, G. M. Stocks, and J. Zhong, arXiv:1412.2528.
[39] N. B. Kopnin, T. T. Heikkilä, and G. E. Volovik, Phys. Rev. B **83**, 220503(R) (2011).
[40] Z. Liu, F. Liu, and Y. S. Wu, Chin. Phys. B **23**, 077308 (2014).
[41] C. Huang, S. Wu, A. M. Sanchez, J. J. Peters, R. Beanland, J. S. Ross, P. Rivera, W. Yao, D. H. Cobden, and X. Xu, Nat. Mater. **13**, 1096 (2014).
[42] Y. Gong, J. Lin, X. Wang, G. Shi, S. Lei, Z. Lin, X. Zou, G. Ye, R. Vajtai, B. I. Yakobson, H. Terrones, M. Terrones, B. K. Tay, J. Lou, S. T. Pantelides, Z. Liu, W. Zhou, and P. M. Ajayan, Nat. Mater. **13**, 1135 (2014).
[43] H. Tian, Z. Tan, C. Wu, X. Wang, M. A. Mohammad, D. Xie, Y. Yang, J. Wang, L. J. Li, J. Xu, and T. L. Ren, Sci. Rep. **4**, 5951 (2014).
[44] A. Koma, J. Cryst. Growth **201–202**, 236 (1999).